

Spatial assessment of femoral neck bone density and microstructure in hip osteoarthritis

Joshua D. Auger^{a,*}, Amartya J. Naik^a, Akira M. Murakami^b, Louis C. Gerstenfeld^b,
Elise F. Morgan^a

^a Boston University, Boston, MA, United States of America

^b Boston University School of Medicine, Boston, MA, United States of America

ARTICLE INFO

Keywords:

Osteoarthritis
Hip
Femur
Imaging
Micro-computed tomography
Bone
Microstructure

ABSTRACT

Osteoarthritis (OA) is known to involve profound changes in bone density and microstructure near to, and even distal to, the joint. Critically, however, a full, spatial picture of these abnormalities has not been well documented in a quantitative fashion in hip OA. Here, micro-computed tomography (44.8 $\mu\text{m}/\text{voxel}$) and data-driven computational anatomy were used to generate 3-D maps of the distribution of bone density and microstructure in human femoral neck samples with early (6F/4M, mean age = 51.3 years), moderate (14F/8M, mean age = 60 years), and severe (16F/6M, mean age = 63.3 years) radiographic OA. With increasing severity of radiographic OA, there was decreased cortical bone mineral density (BMD) ($p=0.003$), increased cortical thickness ($p=0.001$), increased cortical porosity ($p=0.0028$), and increased cortical cross-sectional area ($p=0.0012$, due to an increase in periosteal radius ($p=0.018$)), with no differences detected in the total femoral neck or trabecular compartment measures. No OA-related region-specific differences were detected through Statistical Parametric Mapping, but there were trends towards decreased tissue mineral density (TMD) in the inferior femoral neck with increasing OA severity ($0.050 < p \leq 0.091$), possibly due to osteophytes. Overall, the lack of differences in cortical TMD among radiographic OA groups indicated that the decrease in cortical BMD with increasing OA severity was largely due to the increased cortical porosity rather than decreased tissue mineralization. As porosity is inversely associated with stiffness and strength in cortical bone, increased porosity may offset the effect that increased cortical cross-sectional area would be expected to have on reducing stresses within the femoral neck. The use of high-resolution imaging and quantitative spatial assessment in this study provide insight into the heterogeneous and multi-faceted changes in density and microstructure in hip OA, which have implications for OA progression and fracture risk.

1. Introduction

Osteoarthritis (OA) is a chronic, painful, and currently incurable disease characterized by structural deterioration and loss of function of synovial joints. Originally considered a disease of cartilage alone, OA is now understood to involve the entire joint (Radin et al., 1972; Burr, 2004). Attention has increasingly focused on the role—both biomechanical and biological—that bone in the subchondral (Bobinac et al., 2003; Buckland-Wright, 2004; Hayami et al., 2006) and nearby metaphyseal regions (Dedrick et al., 1993; Messent et al., 2005; Ding et al., 2003) may play in the pathogenesis of OA. Notably, in hip OA, many of the bony abnormalities that are hallmarks of the disease are focal (e.g. osteophytes at joint margins and subchondral bone cysts) (Chiba et al.,

2014; Crema et al., 2010; Rhaney and Lamb, 1955) or occur in an otherwise spatially non-uniform manner (e.g. subchondral plate thickening and decreased mineralization within the trabecular bone) (Neilson et al., 2004; Day et al., 2001; Wang et al., 2016). Broadly speaking, these changes in density and microstructure, because they presumably reflect changes in the local stiffness of the bone tissue, are likely to alter the distribution of stress and strain throughout the proximal femur. These alterations may trigger the aberrant cellular signaling and tissue damage characteristics of OA progression (Radin and Rose, 1986; Chudryk et al., 2012) and modulate risk for additional clinical complications such as hip fracture (Calderazzi et al., 2014; Chan et al., 2014; Aguado-Maestro et al., 2017).

Despite the documented changes that occur in the subchondral and

* Corresponding author at: Department of Mechanical Engineering, Boston University, Boston, MA, United States of America.

E-mail address: jauger@bu.edu (J.D. Auger).

<https://doi.org/10.1016/j.bonr.2021.101155>

Received 24 November 2021; Accepted 30 November 2021

Available online 9 December 2021

2352-1872/© 2021 The Authors.

Published by Elsevier Inc.

This is an open access article under the CC BY-NC-ND license

(<http://creativecommons.org/licenses/by-nc-nd/4.0/>).

metaphyseal bone during hip OA, a thorough spatial picture of the abnormalities in bone density and microstructure has not been established in the human hip. Within the proximal femur, the femoral neck in particular is a site of complex loading, considerable load sharing between cortical and trabecular compartments (Nawathe et al., 2015), and high fracture risk (Fox et al., 2000). Prior studies have found an overall increase in bone volume fraction (BV/TV) in the femoral neck in OA compared to controls (Wang et al., 2016), owing partly to a thicker cortex in the inferior portion (Neilson et al., 2004). Cortical bone mapping (CBM) (Treece et al., 2010; Treece and Gee, 2015) of the proximal femur has found increased cortical thickness in the superior subchondral bone plate and the supero-lateral femoral head-neck junction with increasing severity of OA (Turmezei et al., 2016; Poole et al., 2017). However, OA-related decreases in tissue modulus in trabecular bone (Day et al., 2001) and increases in cortical porosity (Blain et al., 2008) can mitigate the effect of increased bone volume and bone thickness on overall bone stiffness, as can changes in anisotropy of the microstructure (Ding et al., 2003). Altogether, these findings emphasize that OA may be associated with spatially non-uniform changes in multiple features of bone microstructure, including in regions extending beyond the peri-articular bone, in a manner that could alter the load-bearing capability of the proximal femur.

Therefore, the goal of this study was to quantify OA-associated spatial differences in bone density and microstructure within the femoral neck for different stages of severity of radiographic OA. We used micro-computed tomography imaging and custom image processing to measure the density and microstructure of the cortical and trabecular bone from the femoral necks of human donors undergoing elective total hip arthroplasty, which were stratified by Kellgren-Lawrence (KL) grade of OA severity. The first objective was to examine the typically reported compartment-level average measures across early, moderate, and severe radiographic OA. The second objective was to examine the spatial distribution of bone density and microstructure throughout the femoral neck and investigate any regional effects across defined stages of OA progression.

2. Methods

2.1. Specimens

Femoral neck specimens were retrieved from individuals undergoing elective total hip arthroplasty (THA) at Boston Medical Center. The main reason for elective THA was pain and/or lack of mobility that necessitated invasive correction. Specimen collection was performed in accordance with IRB approval from our institution (IRB number H-32517). Review of patient records for individuals over 18 years age and who

were undergoing elective THA at Boston Medical Center was done prior to approaching the individual for potential consent. Patients with sickle cell disease, rheumatoid arthritis, past or current chemotherapy, past or current usage of osteoporosis medications (bisphosphonates, parathyroid hormone, selective estrogen receptor modulators, Denosumab), and past or current usage of cortical steroids or anti-tumor necrosis factor therapy were excluded. We also did not include patients who were cognitively impaired and/or unable to self-consent. Patients were assigned Kellgren-Lawrence (KL) grades (Kellgren and Lawrence, 1957) from pre-op radiographs by a trained radiologist (Boston University School of Medicine, Boston, MA) who was blind to the outcome/nature of the patient condition. Early, moderate, and severe radiographic OA groups were defined as KL-1–KL-2, KL-3, and KL-4 graded specimens, respectively.

The femoral head and neck tissue was excised during THA and was then cut at the head-neck junction to separate the femoral head from the femoral neck (Fig. 1). Some specimens were excluded because an insufficient amount of the femoral neck was present: broken or partial samples ($n = 25$), and thin or wedge-shaped samples less than 1.6 mm thick that would constrain trabecular thickness measures ($n = 9$). After these exclusions, $n = 54$ samples remained (Table 1). To account for variations in the amount of femoral neck retrieved from THA due to cut plane angle, the volume of interest (VOI) for all samples began at the proximal femoral head-neck cut plane (Fig. 1, part A) and extended distally along the axis of the femoral neck, up until the final perpendicular plane to the head-neck cut plane.

2.2. Imaging

Micro-computed tomography (μ CT) scans were performed at a nominal resolution of 44.8 $\mu\text{m}/\text{voxel}$ (Zeiss Xradia 520 Versa; 60 kV, 5 W, 410 ms exposure time). Specimens were immersed in protease-inhibitor (Catalog #A32963, Thermo Scientific) solution during scanning (Wahlquist et al., 2017). A commercially available hydroxyapatite phantom (Scanco Medical, Bruttisellen, Switzerland) was also scanned to provide a linear transform of voxel grayscale intensity to equivalent mineral density (mgHA/ccm).

Table 1
Donor characteristics ($n = 54$). Presented as mean (SD), range.

Samples	n	Age (years)	BMI
Early OA, KL-1–2	10 (6F/4M)	51.3 (15.2), 26–78	29.6 (4.6), 20.9–36.6
Moderate OA, KL-3	22 (14F/8M)	60.0 (9.9), 39–79	30.7 (7.2), 22.7–49.1
Severe OA, KL-4	22 (16F/6M)	63.3 (9.9), 47–83	30.1 (5.1), 21.8–37.9

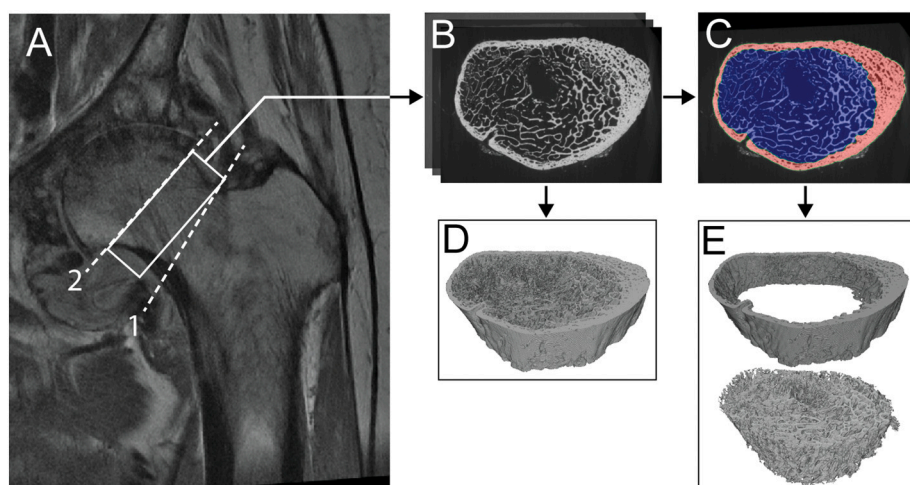


Fig. 1. A representative pre-operative patient MRI scan (part A) demarcates where the femoral head and neck tissue was excised during elective THA (part A, dotted cut plane 1) and then the femoral neck tissue was separated at the femoral head-neck junction (part A, dotted cut plane 2). The VOI (part A, white box) underwent micro-computed tomography scanning, resulting in a stack of grayscale images (part B). The cortical and trabecular compartments were then segmented in ImageJ (part C). A 3-D render of the entire femoral neck sample (part D) and the cortical (part E, top) and trabecular (part E, bottom) compartments are also shown.

2.3. Image processing

The μ CT data were exported as grayscale image stacks and were semi-automatically segmented into trabecular and cortical compartments using custom scripts in ImageJ (Schindelin et al., 2012) that were written based on published methods (Fig. 1) (Buie et al., 2007; Burghardt et al., 2010). A trained operator ran the semi-automated image segmentation scripts and made manual corrections where necessary, especially those specimens that corresponded to late stages of osteoarthritis with osteophytes and cortical “trabecularization” (Fig. 2). To assess reliability, a sub-set of specimens were previously analyzed using commercially available Scanco visualization and analysis software (Scanco Medical, Bruttisellen, Switzerland) and paired *t*-tests of the results found no difference between the ImageJ custom scripts and Scanco analysis ($p \geq 0.223$ for all measures, see Supplementary Table 1). To assess repeatability, a sub-set of specimens was analyzed by two independent operators and intra-class correlation coefficient (ICC) showed no difference between operators ($ICC \geq 0.991$ for all measures), as well as no difference found from paired *t*-tests between operator results ($p \geq 0.099$ for all measures, see Supplementary Table 2). The operator performing image analysis was blinded to both KL scores and clinical and functional information. Measures of bone density and microstructure were calculated using custom ImageJ scripts and the BoneJ plugin (Doube et al., 2010), and included: trabecular thickness (Tb.Th*), trabecular separation (Tb.Sp*), cortical “cortex” thickness (Ct.Th, defined as the mean sphere-fit within the cortical compartment (cortex) with pores filled in, or simply, the nominal difference between the outer periosteal radius and inner endosteal radius), cortical bone tissue thickness (Cb.Th, defined as the mean sphere-fit of the cortical bone tissue with pores present), cortical separation (Ct.Sp), and cortical porosity (Ct.Po), as well as bone volume fraction (BV/TV), bone mineral density (BMD, defined as the mean density value of all voxels in a given region), tissue mineral density (TMD, defined as the mean density value of bone tissue voxels in a given region), and cross-sectional area (CSA) for the total femoral neck, trabecular compartment (Tb), and cortical (Ct) compartment (referred to as the cortex). To help interpret any differences in CSA for an irregularly shaped anatomy, the total CSA and trabecular CSA were used to calculate the effective outer periosteal (R. Peri) and inner endosteal (R. Endo) radius, respectively, of the femoral neck cortex, assuming a circular cross-section.

2.4. Spatial maps

Spatial maps were created for the purpose of quantifying spatial variation in the aforementioned measures of density and microstructure throughout the femoral neck (Poole et al., 2017; Marques et al., 2018;

Treece et al., 2015). A common femoral neck template, i.e. a canonical femoral neck shape, was determined as the average of all femoral neck shapes present in the study (Fig. 3). A volumetric mesh was prescribed to the femoral neck template (mean element side length = 0.98 mm) and then underwent mesh-morphing (IA-FEMesh, The University of Iowa, Iowa City, IA) to morph onto each femoral neck sample. A series of affine transformations were used to (i) orient the top surface of the template mesh with the femoral head-neck cut-plane of the femoral neck specimen, (ii) align the centroid of the template mesh with the centroid of the specimen, and (iii) uniformly scale the entire mesh to fit the overall scale of the specimen. Then, the edges of the mesh were prescribed an initial manual deformation in the transverse cross-sectional plane to fit the edges of the specimen, which was then refined through closest point projection to the outer surface (IA-FEMesh, The University of Iowa, Iowa City, IA). This step brings all femoral neck specimens, and their spatial distributions of density and microstructure, onto a common, 3-D anatomic reference model mesh. Each of the aforementioned measures of bone density and microstructure (BV/TV, BMD, TMD, thickness (from sphere-fitting of the bone tissue), and separation/porosity (from sphere-fitting of the negative, non-bone space)) were then evaluated within a 4 mm cubic sub-region centered around each node in the mesh for each femoral neck specimen (ImageJ through the Boston University Shared Computing Cluster, Holyoke, MA), following prior study methods for mapping continuum-level measures onto a finer resolution mesh (Unnikrishnan and Morgan, 2011). For this step, the spatial sub-region assessments of bone density and microstructure were restricted by the given compartment (cortical or trabecular) in which the sub-region centroid resided. This ensures that the local sub-regions of the cortex and trabecular compartment are only compared to the corresponding locations in the cortex and trabecular compartment of other specimens, respectively. The presence of an osteophyte in one of these cortical sub-regions does affect the measured values of density and microstructure in this sub-region, and hence these differences are inherently included in our comparison of these measures among OA groups. We note that for these maps, therefore, cortical porosity in each cubic sub-region is defined as separation. These data were then represented on the common femoral neck template according to the inverse of the deformations applied during the initial mesh morphing step (Fig. 3) (Marques et al., 2018; Carballido-Gamio et al., 2013).

2.5. Statistical analysis

2.5.1. Age, sex, and BMI comparisons

All age, sex, and BMI comparisons were conducted in JMP software (v15.0.0, SAS Institute Inc., Cary, NC). Non-parametric analysis of variance (ANOVA) and Wilcoxon post hoc tests were used to assess

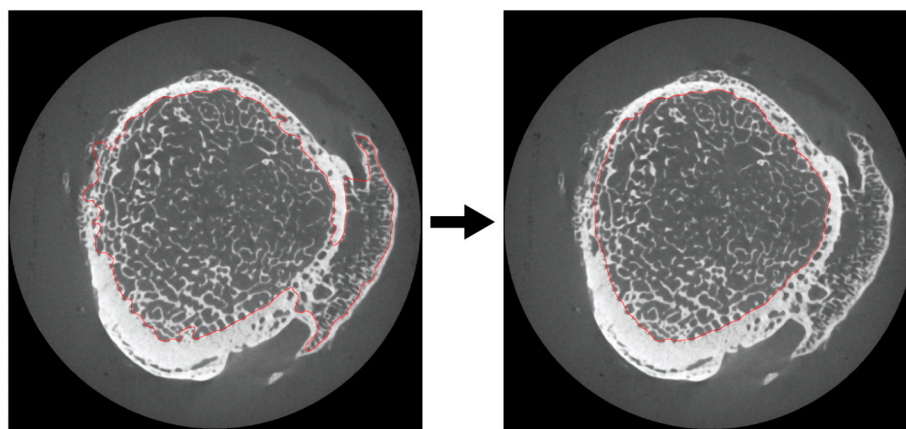


Fig. 2. A representative μ CT slice of the femoral neck where the initial contouring results (in red) of the automated segmentation script (left) necessitated manual correction (right) by a trained operator, thus all segmentation was performed in a semi-automated fashion.

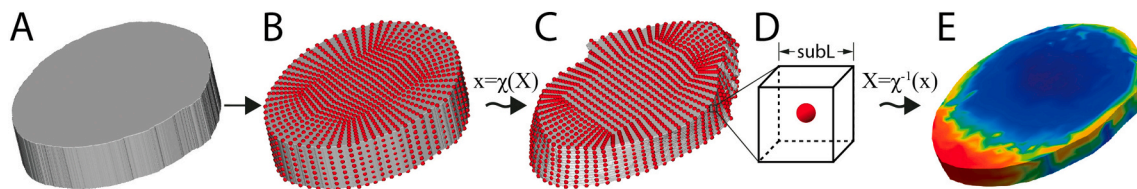


Fig. 3. The canonical femoral neck template (A), defined as the average of all femoral neck shapes present, was ascribed a mesh (B, mean element side length = 0.98 mm) that was then morphed onto each individual femoral neck sample (C) (IA-FEMesh, The University of Iowa, Iowa City, IA). Cubic sub-regions (subL = 4 mm) centered around each node (D) were evaluated for each measure of bone density and microstructure using ImageJ, the results of which were mapped back onto the anatomic reference model (E) and visualized in ParaView (v5.9.0, Kitware Inc., New York, NY).

whether there were differences in age among OA groups. The two youngest donors (26 and 31 years old) in the cohort, while still electing for THA due to pain and/or lack of mobility, did qualify as two outliers. Therefore, this statistical analysis was performed before and after excluding the two outliers. A Pearson's chi-squared test was used to check for differences among radiographic OA groups in the distribution of males vs. females. Non-parametric ANOVA was used to assess whether there were differences in BMI among radiographic OA groups.

2.5.2. Compartment-level statistics

All compartment-level statistics were conducted in JMP software (v15.0.0, SAS Institute Inc., Cary, NC). Non-parametric ANOVA was used to assess differences in measures of bone density and microstructure of the total femoral neck, cortical compartment, and trabecular compartment among radiographic OA groups. The significance level was set at 0.05, with a Bonferroni correction applied to account for multiple comparisons for measures of the total femoral neck ($p_{adjusted}=0.013$), trabecular compartment ($p_{adjusted}=0.008$), and cortical compartment ($p_{adjusted}=0.006$). When differences among radiographic OA groups were found, a non-parametric Wilcoxon of each pair was conducted as a post hoc test to identify between which OA groups the differences existed.

To check whether any observed density or microstructure differences among radiographic OA groups were confounded by age, sex, or BMI, we used a general linear model with age, sex, BMI, and OA group as independent variables to assess whether there were any effects of age, sex, or BMI, or any interaction effects between age, sex, or BMI and OA group for all of the aforementioned compartment-level measures. Additionally, we re-ran the non-parametric ANOVAs of each measure after excluding the two outliers in age, to clarify whether OA-related differences persisted.

2.5.3. Statistical parametric mapping

Statistical Parametric Mapping (SPM) was implemented in MATLAB (R2020a, MathWorks, Natick, MA) using the `spm1d` package (Pataky, 2010) to assess whether the spatial distribution of any of the measures of bone density or microstructure differed among radiographic OA groups. In SPM, a general linear model is used to estimate parameters that could explain spatially continuous data. Gaussian random field theory is then used to resolve multiple comparisons that result from making inferences over a volume, controlling the overall chance of false positives (Pataky, 2016). This process enables the generation of one-way non-parametric ANOVA statistical maps of the femoral neck indicating regionally specific effects (Pataky, 2010; Friston et al., 1991). Significance level was set at 0.05. Follow-up SPM was conducted with significance level at 0.1 to identify any trends in measures of density and microstructure.

3. Results

3.1. Age, sex, and BMI differences

There was no difference in distribution of BMI among OA groups ($p=0.955$). There was no difference in distribution of males vs. females among OA groups ($p=0.721$). There was a difference in age between the

early and severe radiographic OA groups ($p=0.015$, mean age = 51.3 and 63.3 years, respectively). Excluding the two outliers eliminated the difference in age between the early and severe radiographic OA groups ($p=0.074$, adjusted mean age = 57.0 and 63.3 years, respectively).

3.2. Compartment-level measures

Differences in measures of bone density and microstructure among OA groups were found in the cortical ($p_{adjusted}=0.006$) but not trabecular compartment (Table 2). With increasing radiographic OA severity, Ct. BMD decreased ($p=0.003$), and Ct.Th ($p=0.001$), Ct.Sp ($p=0.005$), Ct.Po ($p=0.003$), and Ct.CSA ($p=0.001$) increased (Fig. 4), and a trend towards decreased Ct.BV/TV ($p=0.011$). No differences were found in any measures of the total femoral neck ($p \geq 0.025$, where $p_{adjusted}=0.013$) or trabecular compartment ($p \geq 0.377$, where $p_{adjusted}=0.008$) across radiographic OA groups. The general linear model showed no association between any compartment-level measure and age ($p \geq 0.344$) and no interaction effect between age and OA group ($p \geq 0.051$, where $p_{adjusted}=0.013$). Even after excluding the two youngest specimens, Ct. BMD decreased ($p=0.002$) and Ct.Po increased ($p=0.005$) with increased OA severity, with trends towards decreased Ct.Sp ($p=0.010$) and increased Ct.Th ($p=0.011$) and Ct.CSA ($p=0.009$). For these compartment-level measures, no effect of age ($p \geq 0.420$) or sex ($p \geq 0.201$) or BMI ($p \geq 0.667$) and no interaction effect of age and OA group ($p \geq 0.061$) or sex and OA group ($p \geq 0.393$) or BMI and OA group ($p \geq 0.528$) was found.

The increase in Ct.Th and Ct.CSA stemmed primarily from an increase in periosteal radius with increasing OA severity (R.Peri $p=0.018$, Table 3, Fig. 5). For the early, moderate, and severe radiographic OA groups, Non-parametric Wilcoxon of each pair identified difference in R. Peri between the early and severe radiographic OA groups ($p=0.017$), but no other severity group pairings ($p \geq 0.108$). There was no difference in endosteal radius (R.Endo, $p=0.395$) across OA groups.

3.3. Spatial distribution and SPM

The 3-D spatial maps revealed heterogeneity in measures of density and microstructure throughout the femoral neck within each radiographic OA severity group (Fig. 6, columns 1–3). No region-specific differences in spatial distribution were found among OA severity groups (Fig. 6, column 4, $\alpha=0.05$) as evident by the $F_{critical}$ values being higher than the maximum F-values observed for each measure. However, trends ($0.05 \leq p \leq 0.1$) towards decreased TMD with increasing radiographic OA severity in two sub-regions of the infero-posterior cortex ($p=0.050$) and infero-anterior cortex ($p=0.091$) were observed (Fig. 6, column 4, marker for $\alpha=0.1$).

4. Discussion

The goal of this study was to quantify OA-related spatial differences in bone density and microstructure within the femoral neck. Compartment-level measures revealed decreased bone mineral density, increased thickness, increased porosity, and increased cross-sectional

Table 2

Compartment-level measures (mean (SD), range) of femoral neck density and microstructure across radiographic OA severity groups with *p*-values from non-parametric ANOVA. A Bonferroni correction was applied to account for multiple comparisons for measures of the total femoral neck (*p*_{adjusted}=0.013), trabecular compartment (*p*_{adjusted}=0.008), and cortical compartment (*p*_{adjusted}=0.006).

Measures	Early OA	Moderate OA	Severe OA	p-Value
Total femoral neck				
BV/TV (–)	0.383 (0.090), 0.243–0.507	0.402 (0.097), 0.246–0.601	0.375 (0.097), 0.255–0.671	0.578
BMD (mgHA/ccm)	404.8 (88.9), 230.4–508.7	410.0 (83.9), 240.6–560.7	370.6 (85.7), 191.2–607.1	0.263
TMD (mgHA/ccm)	731.8 (67.8), 585.5–800.7	724.4 (52.3), 610.6–784.1	690.4 (89.3), 423.1–762.4	0.166
CSA (mm ²)	706.9 (92.6), 564.4–866.9	791.4 (133.6), 586.8–1025.6	880.5 (197.3), 547.4–1289.5	0.025
Trabecular (Tb) compartment				
Tb.BV/TV (–)	0.221 (0.086), 0.059–0.352	0.210 (0.081), 0.042–0.405	0.204 (0.101), 0.069–0.525	0.535
Tb.BMD (mgHA/ccm)	290.1 (73.1), 178.4–392.4	281.6 (64.8), 116.9–425.2	261.1 (86.0), 121.2–490.3	0.414
Tb.TMD (mgHA/ccm)	612.3 (39.7), 527.9–664.8	606.0 (42.9), 508.1–685.8	591.9 (79.9), 352.8–674.3	0.894
Tb.Th (mm)	0.279 (0.042), 0.217–0.372	0.277 (0.045), 0.188–0.368	0.289 (0.071), 0.221–0.549	0.989
Tb.Sp (mm)	1.013 (0.679), 0.601–2.918	0.812 (0.147), 0.464–1.171	0.931 (0.342), 0.257–1.702	0.531
Tb.CSA (mm ²)	544.2 (108.0), 398.9–763.8	534.4 (124.7), 385.7–811.7	592.8 (169.4), 341.8–1022.8	0.377
Cortical (Ct) compartment				
Ct.BV/TV (–)	0.853 (0.059), 0.749–0.912	0.774 (0.135), 0.421–0.905	0.729 (0.134), 0.482–0.942	0.011
Ct.BMD (mgHA/ccm)	785.5 (83.5), 612.3–862.2	691.9 (124.6), 371.9–846.3	651.9 (114.4), 442.5–855.6	0.003
Ct.TMD (mgHA/ccm)	831.7 (66.3), 684.7–893.1	796.2 (63.6), 627.2–889.3	774.6 (55.7), 675.3–879.6	0.024
Ct.Th (mm)	2.339 (0.330), 1.148–3.538	3.473 (0.222), 1.378–6.421	3.768 (0.223), 1.950–6.553	0.001
Cb.Th (mm)	1.343 (0.415), 0.666–2.135	1.462 (0.451), 0.716–2.219	1.135 (0.401), 0.542–2.021	0.049
Ct.Sp (mm)	0.356 (0.095), 0.217–0.530	0.656 (0.331), 0.259–1.711	0.725 (0.436), 0.216–1.751	0.005
Ct.Po (–)	0.067 (0.042), 0.017–0.128	0.161 (0.124), 0.034–0.410	0.217 (0.154), 0.010–0.509	0.003
Ct.CSA (mm ²)	150.2 (38.9), 88.3–221.2	235.2 (61.9), 106.3–340.5	270.7 (125.9), 101.1–620.9	0.001

area of the cortex with increasing radiographic OA severity. In contrast, there were no differences found in total femoral neck measures, or in measures of the trabecular compartment. Additionally, while the spatial maps showed heterogeneity of density and microstructure within each compartment and overall throughout the femoral neck (Fig. 6), these variations were relatively consistent among radiographic OA groups. No OA-related region-specific effects were found other than a trend ($0.05 \leq p \leq 0.1$) towards decreased TMD with increasing OA severity in the inferior cortex of the femoral neck. The results of this study indicate that OA-related differences in bone occur in distal metaphyseal regions of the hip, not just in subchondral areas, and that the decline in Ct.BMD with increasing OA severity is largely a manifestation of differences in porosity rather than in the mineral content of the tissue itself. These data suggest that OA-related decreases in cortex density (i.e. lower Ct.BMD and higher Ct.Po) may offset the effects of increases in overall size (i.e. Ct.Th, Ct.CSA, and R.Peri) on distributions of stress within, and overall structural integrity of, the femoral neck.

This is the first study to combine spatial maps and SPM to test for

region-specific differences in bone density and microstructure across disease severity in hip OA. Although numerous studies have compared bone density and microstructure between hip OA and non-OA (e.g. osteoporotic) cohorts (Neilson et al., 2004; Wang et al., 2016; Rubinacci et al., 2012; Boutroy et al., 2011), our investigation focused *within* OA in order to identify differences in the parameters among early, moderate and severe stages. We focused on the femoral neck, despite its location distal to the articulating joint, because of reports of OA-related effects in this region (Neilson et al., 2004; Wang et al., 2016; Djuric et al., 2013) and because of the susceptibility of this region to fracture (Fox et al., 2000; Johannesdottir et al., 2011; Bell et al., 1999a). While OA is generally thought to be inversely associated with fracture (Rubinacci et al., 2012; Pedersen et al., 1987; Sugano et al., 2020), recent studies are challenging the idea that OA is protective against fracture (Chudyk et al., 2012; Chan et al., 2014), suggesting that OA may instead alter which regions of the proximal femur are at risk (Calderazzi et al., 2014; Aguado-Maestro et al., 2017; Wolf et al., 2009). Within the proximal femur, the primary compressive group is the main conduit of load from acetabular-femoral contact, through the femoral head, to the inferior femoral neck cortex (Neilson et al., 2004). Thus, OA-related differences in the femoral neck cortex can indicate the extent to which OA alters load transmission through the proximal femur. The data-driven computational anatomy approach used here provides insight into the spatial heterogeneity of OA-related femoral neck cortical porosity, thickness, and TMD independently, where lower-resolution imaging assessments would lump all these measures together as BMD. Here, decreased Ct.BMD, but a lack of difference in TMD, suggests that the reported change in density is mainly a result of microstructural differences (e.g. Ct.Po) as opposed to changes in mineralization (e.g. TMD).

This study has a number of limitations to be considered. First, the recruitment strategy for tissue specimens from elective THA was not conducive to including a non-OA group for comparison. While prior studies have used tissue from hip fracture patients (non-elective THA) as a control group, because our study required that the femoral neck be intact, hip fracture cases were not a viable control group for this study. While cadaver tissue is another potential option, it was not possible to obtain matching donor characteristics (age, race, ethnicity, weight, BMI) in a reasonable amount of time. We, therefore, opted to forgo a non-OA comparison group or control group and instead focused the goal of this study on examining differences *among* severity levels of OA. This means that the differences among radiographic OA groups could be due to other factors, such as aging. However, there were no effects of age and no interaction between age and radiographic OA group; further, differences in density and microstructure among OA groups persisted after exclusion of the age outliers. Another limitation is that the early radiographic OA patients in this study, while being assigned a radiographic OA score of KL-1–KL-2, did still undergo elective THA due to pain and/or lack of mobility, and therefore, may not be representative of the non-surgical early OA population. Another limitation is that this study did not exclude osteophytes from specimen analysis and thus, the semi-automated image segmentation required a final check by a trained user for manual adjustments to ensure correct identification of the endosteal boundary and not classify osteophytes or trabecularized cortex regions as part of the trabecular compartment; therefore, osteophytes, when present, were considered part of the cortex (Fig. 2). Osteophytes are an established feature of OA, and excluding them would both reduce the scope of the characterization and incorrectly assume that the density and microstructure (including cortical thickness) of the rest of the femoral neck are independent of the presence of osteophytes. Osteophytes tend to accumulate around the inferior periphery of the femoral head-neck junction (Turmezei et al., 2014) and are a defining feature for higher KL grades ascribed to increasing severity of OA; hence, osteophytes could explain, in part, the region-specific trend towards decreased TMD in the inferior portion of the femoral neck found here and by others (Rubinacci et al., 2012).

Furthermore, a key limitation of the SPM analysis was the inability to

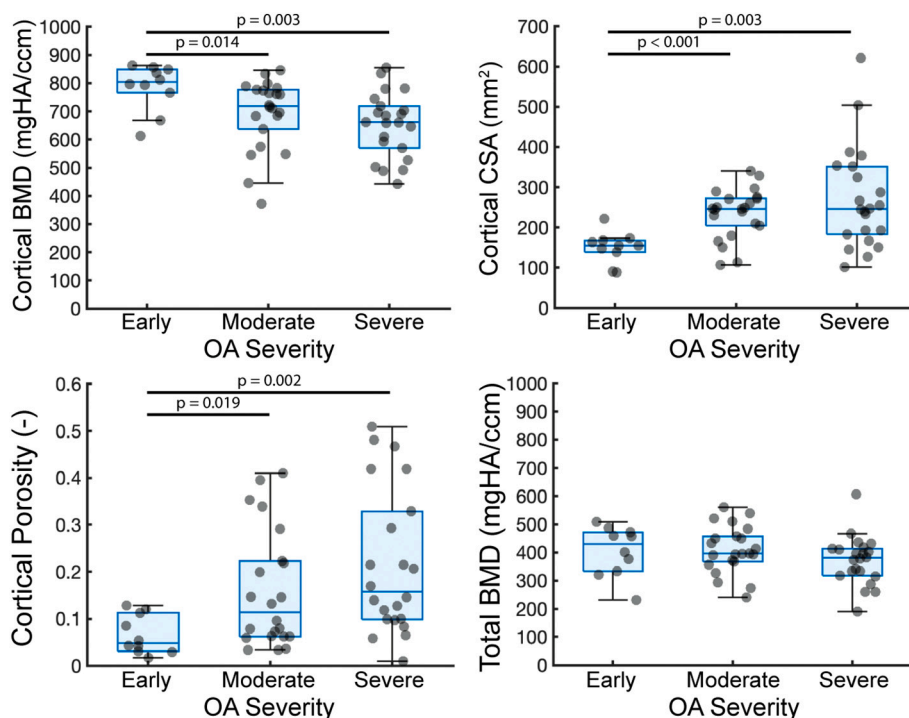


Fig. 4. Non-parametric ANOVA with Bonferonni correction revealed differences in cortical compartment measures Ct.BMD, Ct.Po, and Ct.CSA across early, moderate, and severe radiographic OA. In contrast, no differences were found in any total or trabecular measures. Pairwise differences from non-parametric Wilcoxon of each pair are noted.

Table 3
Cortex size across radiographic OA groups. Presented as mean (SD), range.

Measures	Early OA	Moderate OA	Severe OA
Ct.CSA (mm ²)	150.2 (38.9), 88.3–221.2 ^{*†}	235.2 (61.9), 106.3–340.5 [*]	270.7 (125.9), 101.1–620.9
Ct.Th (mm)	2.339 (0.330), 1.148–3.538 ^{*†}	3.473 (0.222), 1.378–6.421 [*]	3.768 (0.223), 1.950–6.553
R.Peri (mm)	14.97 (0.98), 13.4–16.6 [†]	15.82 (1.32), 13.7–18.1	16.64 (1.87), 13.2–20.2 [†]
R.Endo (mm)	13.11 (1.28), 11.3–15.6	12.96 (1.46), 11.1–16.1	13.62 (1.87), 10.4–18.0
Ct.BMD (mgHA/ccm)	785.5 (83.5), 612.3–862.2 ^{*†}	691.9 (124.6), 371.9–846.3 [*]	651.9 (114.4), 442.5–855.6 [†]

^{*} Denotes paired difference between early and moderate OA for that measure.
[†] Denotes paired difference between early and severe OA for that measure.

run a general linear model accounting for covariates. The current *spm1d* package offers a general linear model, but does not allow for corrections of unequal variance, while the non-parametric ANOVA does. In this cohort of specimens, the variance ratio ≥ 2 in 44.3%, 46.4%, 49.0%, 78.9%, and 73.4% of the femoral neck mesh for BV/TV, BMD, TMD, thickness, and separation, respectively, across OA groups. Given unequal variance, and the initial assessment of covariates for compartment-level results that found no interaction effects of age, sex, or BMI, the most appropriate statistical test in the SPM analyses was a non-parametric ANOVA, despite not including covariates. Another limitation of the SPM analysis was the low statistical power for the given number of samples and measured effect size. An ad-hoc power assessment of SPM was conducted by doing multiple re-runs of SPM, where each run was performed on a random selection of specimens from within the study cohort. The maximum power within the spatial mesh was 22%, 48%, 56%, 46%, and 26% for each measure of BV/TV, BMD, TMD, thickness, and separation, respectively. Thus, there was not enough statistical power to detect differences at the measured effect size with SPM. While additional samples would increase statistical power, we note

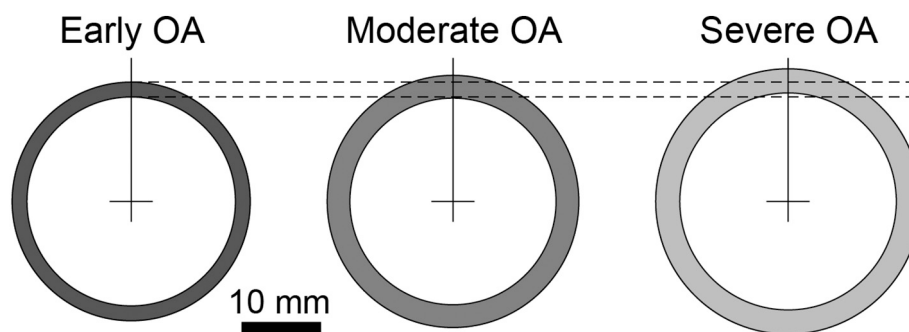


Fig. 5. Schematic representations of the mean effective periosteal and endosteal radii of the femoral neck by radiographic OA groups. The dotted lines denote the periosteal and endosteal radii of the early radiographic OA group for reference. The grayscale shading reflects the difference in Ct.BMD across OA groups. Periosteal radius was different between early and severe OA groups ($p=0.0174$), while no difference was detected in endosteal radius.

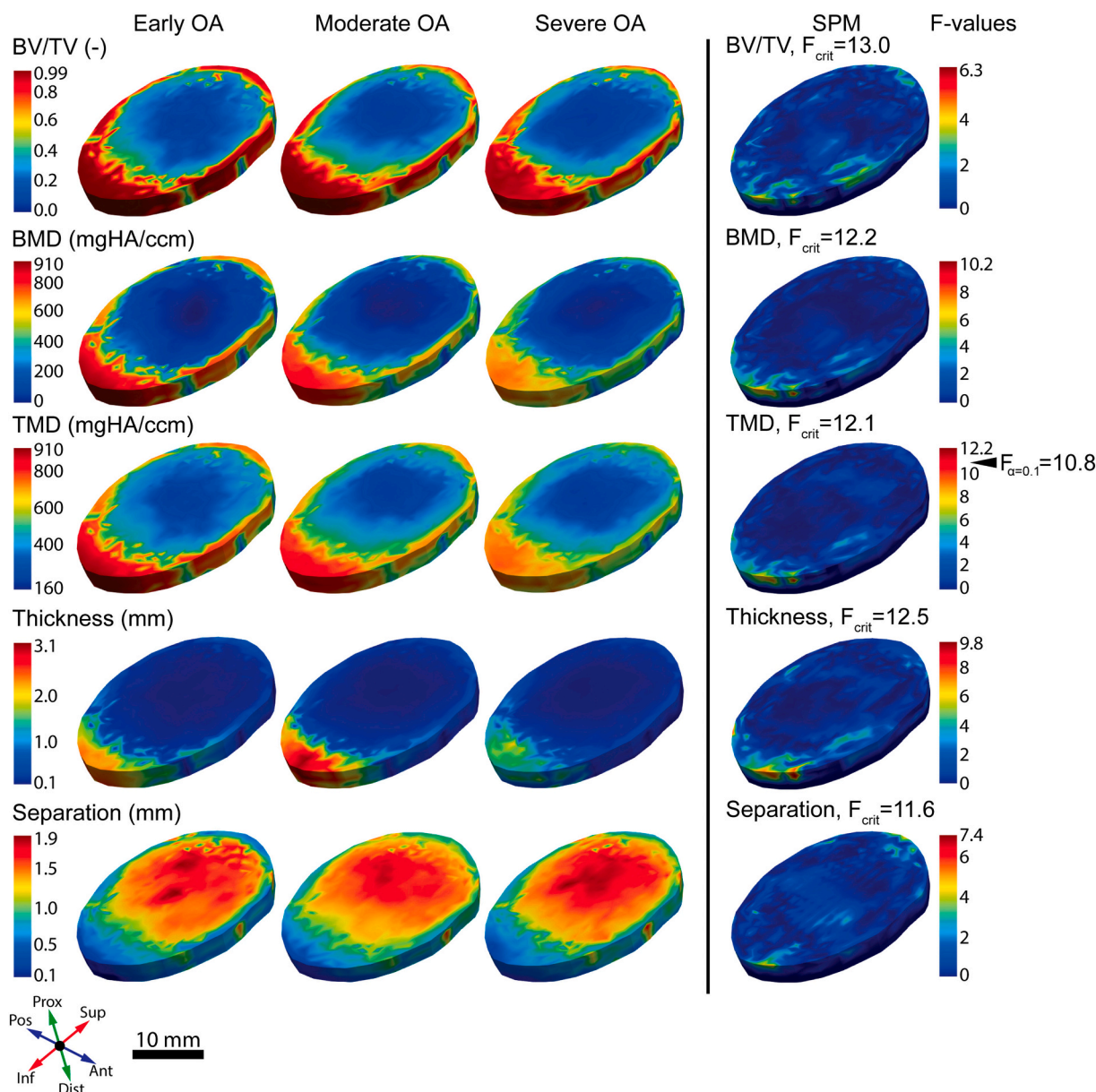


Fig. 6. 3-D spatial maps of median values of each measure of density and microstructure for early (column 1), moderate (column 2), and severe (column 3) radiographic OA groups. Spatial maps of F-values from SPM (column 4) for each measure show no significant regional effects for any measure ($F_{critical}$ for $\alpha=0.05$ specified for each measure). To identify trending regions in TMD, $F_{critical}$ for $\alpha=0.1$ is labeled on the color scale. Anatomical orientation and scale bar in the bottom left corner.

that the 3-D spatial maps of each measure reveal that there is a similar overall spatial pattern of density and microstructure for each OA group. Therefore, our interpretation is that the distributions are qualitatively similar and that a large number of samples would be needed to detect the relatively small differences in spatial distribution among OA groups. Also, it is important to note that this study is a cross-sectional study and thus, we cannot infer causality or the direction of any effects. Just as it is conceivable that altered loading of the hip, possibly due to patient compensation for lack of mobility or pain avoidance, may lead to changes in bone density and microstructure in the osteoarthritic femur, it is also possible that alterations in loading caused by other factors, such as cam morphology and hip dysplasia (Thomas et al., 2014; Agricola et al., 2013; Saberi Hosnijeh et al., 2017; Ganz et al., 2003), which are associated with elevated risk of OA, may cause these bone changes. To fully characterize the spatio-temporal progression of OA, both scenarios warrant further investigation.

When looking across OA severity groups, we found no differences in BV/TV. However, prior studies have reported increased Tb.BV/TV (Wang et al., 2016; Blain et al., 2008; Rubinacci et al., 2012; Boutroy et al., 2011) and Ct.BV/TV (Neilson et al., 2004; Rubinacci et al., 2012) in the femoral neck when comparing OA to non-OA. This contrast in findings could be, in part, due to prior studies comparing OA to non-OA, whereas the goal of this study was to examine differences *within* OA as disease severity increases. This contrast may be a reflection of the incremental, spatiotemporal pathogenesis of OA (Chen et al., 2018) where bone changes between stages of disease progression (i.e. across OA severity groups) may not be readily perceptible, but are apparent when lumping and comparing an OA cohort to a non-OA benchmark. Additionally, our study is the first to report decreased cortical BMD, as measured by μ CT imaging, with increasing OA severity. This is in contrast to a prior study that found increased total aBMD in OA compared to osteoporosis (OP) (Blain et al., 2008) and another that

found high bone mass was associated with worsening hip OA (Hartley et al., 2021). This contrast could be, in part, due to prior studies using DXA imaging to measure density, which does not distinguish between trabecular and cortical compartments and provides only a single 2-D projection of a 3D object. Increased aBMD, as measured by DXA, could simply reflect an overall increase in femoral neck geometry, which is supported by the increased Ct.Th, Ct.CSA, and R.Peri found here as well as prior studies reporting increased femoral neck width (Blain et al., 2008; Javaid et al., 2009). Notably, the values of R.Peri we found in the present study match those in literature (Beck et al., 1992; Beck et al., 2000). We found no difference in Tb.CSA or endosteal radius with increasing radiographic OA, adding to the ambiguity of conflicting prior reports on whether the size of the trabecular compartment decreases (Wang et al., 2016) or increases (Jordan et al., 2003) in OA as compared to non-OA. Part of this discrepancy may stem from the difficulty of defining the endosteal boundary, both in histology (Blain et al., 2008) and image segmentation (Zebaze et al., 2013), within specimens of a disease that has a marked pathology of altered bone remodeling that may exacerbate age-related cortical “trabecularization” (Bala et al., 2015; Cooper et al., 2007).

Numerous prior studies have reported increased cortical thickness when comparing OA to non-OA (Neilson et al., 2004; Turmezei et al., 2016; Rubinacci et al., 2012; Boutroy et al., 2011), where cortical thickness was defined as a measure of “cortex” thickness, that is the nominal difference between the outer periosteal surface and the inner endosteal boundary, ignoring cortical pores. Our findings here of increased Ct.Th and Ct.CSA, alongside increased R.Peri (while no change in R.Endo), are consistent with the increased cortical “cortex” thickness and increased femoral neck width from prior studies. The increase in thickness may be an indication of the reactivation of cellular processes associated with bone apposition on the periosteal surface that eventually leads to the formation of osteophytes in OA (van der Kraan and van den Berg, 2007; Goldring, 2008), which could be in response to altered stress and strain distributions within the tissue or could be a hyper-inflammatory response within the etiology of OA. Within the cortical compartment, we applied a sphere-fitting technique (Doube et al., 2010), the same that is used to measure trabecular thickness and which recognizes internal pore spaces, to provide a more strictly defined measure of the thickness of the cortical bone tissue within the cortex (denoted as Cb.Th). We found no differences in this measure of thickness, which suggests that the increase in Ct.Po did not outpace that in Ct.Th and Ct.CSA; if it had, then the cortical bone tissue thickness would have decreased. Trabecular thickness changes in OA are less clear as some report no difference (Djuric et al., 2013), consistent with our finding, while others report increased trabecular thickness (Jordan et al., 2003) between OA and non-OA.

The increase in Ct.Po in OA is consistent with prior studies (Blain et al., 2008; Rubinacci et al., 2012; Boutroy et al., 2011; Jordan et al., 2003). Increased porosity within the cortex could be due to heightened remodeling rates triggered by accumulation of microdamage in the form of microcracks, likely a result of mechanical overload characteristic of OA (Burr, 2004; Mori and Burr, 1993). Indeed, there is prior evidence of increased damage volume fraction (Fazzalari et al., 2002) and heightened metabolic activity (Mansell and Bailey, 1998) along the primary compressive group, distal to the affected joint, in hip OA. Resorption spaces develop to remove the cracks and repair the damage with new tissue, creating secondary Haversian canals. Concurrently, increased remodeling on the inner endosteal surface may further exacerbate age-related cortical “trabecularization”, whereby focal expansion of existing canal walls forms “type II” osteons and eventually leads to the coalescence of these large porous spaces (Bala et al., 2015; Cooper et al., 2007; Tomes and de Morgan, 1853). Lastly, proliferation of periosteal cells and reactivation of endochondral ossification gives rise to the formation of porous bony outgrowths (i.e. osteophytes) (van der Kraan and van den Berg, 2007; Goldring, 2008). These resorption spaces and bony outgrowths thus manifest as increased cortical porosity (Bala et al.,

2015; Cooper et al., 2016). Porosity in the cortex is of interest because porosity is a main determinant of the strength and stiffness of cortical bone (Neil Dong et al., 2004; Wachter et al., 2002), and because for much of the length of the femoral neck, the cortex supports the majority of the load in stance phase of gait (Nawathe et al., 2015). Thus, changes in Ct.Po can have a more pronounced impact on overall structural integrity than an equivalent change in size (Schaffler and Burr, 1988; Currey, 1988), and can inhibit the ability of the cortical shell to withstand stresses associated with a fall (Bell et al., 1999a; Bell et al., 1999b; Mccalden et al., 1993).

In conclusion, the findings of this study show that spatially non-uniform, OA-related differences in bone density and microstructure extend distal to the joint surface into the femoral neck, a region of complex loading and known high fracture risk. We have also shown that high-resolution imaging modalities and imaging assessment tools can discern OA-related differences in individual measures of microstructure and mineralization that lower-resolution imaging methods used previously had detected as density. With increasing radiographic OA severity there was decreased Ct.BMD (owing to increased Ct.Po) and increased Ct.Th and Ct.CSA (owing to increased outer periosteal radius), two competing effects in regards to consequences for the stiffness and strength of the femoral neck. The net extent to which these OA-associated differences in bone alter load transmission in the proximal femur requires further investigation. Overall, the spatial assessment tools implemented here provide a method to independently characterize the non-uniform differences in density and microstructure in OA, which have implications for OA progression and fracture risk.

Acknowledgements

NIH AR071657; OREF 17-005; CTSA grant 1UL1TR001430; BU MicroCt Imaging Core Facility; NSF CBET 1429068

Appendix A. Supplementary data

Supplementary data to this article can be found online at <https://doi.org/10.1016/j.bonr.2021.101155>.

References

- Agricola, R., Heijboer, M.P., Bierma-Zeinstra, S.M., Verhaar, J.A., Weinans, H., Waarsing, J.H., 2013. Cam impingement causes osteoarthritis of the hip: a nationwide prospective cohort study (CHECK), 72, 918–923.
- Aguado-Maestro, I., Panteli, M., García-Alonso, M., García-Cepeda, I., Giannoudis, P.V., 2017. Hip osteoarthritis as a predictor of the fracture pattern in proximal femur fractures. *Injury* 48, S41–S46.
- Bala, Y., Zebaze, R., Seeman, E., 2015. Role of cortical bone in bone fragility.
- Beck, T.J., Ruff, C.B., Scott, W.W., Plato, C.C., Tobin, J.D., Quan, C.A., 1992. Sex differences in geometry of the femoral neck with aging: a structural analysis of bone mineral data. *Calcif. Tissue Int.* 50, 24–29.
- Beck, T.J., Looker, A.C., Ruff, C.B., Sievanen, H., Wahner, H.W., 2000. Structural trends in the aging femoral neck and proximal shaft: analysis of the third national health and nutrition examination survey dual-energy X-ray absorptiometry data. *J. Bone Miner. Res.* 15, 2297–2304.
- Bell, K.L., Loveridge, N., Power, J., Garrahan, N., Stanton, M., Lunt, M., Meggitt, B.F., Reeve, J., 1999. Structure of the femoral neck in hip fracture: cortical bone loss in the inferoanterior to superoposterior axis. *J. Bone Miner. Res.* 14, 111–119.
- Bell, K.L., Loveridge, N., Power, J., Garrahan, N., Meggitt, B.F., Reeve, J., 1999. Regional differences in cortical porosity in the fractured femoral neck. *Bone* 24, 57–64.
- Blain, H., Chavassieux, P., Portero-Muzy, N., Bonnel, F., Canovas, F., Chammass, M., Maury, P., Delmas, P.D., Rizzoli, R., 2008. Cortical and trabecular bone distribution in the femoral neck in osteoporosis and osteoarthritis. *Bone* 43, 862–868.
- Bobinac, D., Spanjol, J., Zoricic, S., Maric, I., 2003. Changes in articular cartilage and subchondral bone histomorphometry in osteoarthritic knee joints in humans. *Bone* 32, 284–290.
- Boutroy, S., Vilayphiou, N., Roux, J.-P., Delmas, P.D., Blain, H., Chapurlat, R.D., Chavassieux, P., 2011. Comparison of 2D and 3D bone microarchitecture evaluation at the femoral neck, among postmenopausal women with hip fracture or hip osteoarthritis. *Bone* 49, 1055–1061.
- Buckland-Wright, C., 2004. Subchondral bone changes in hand and knee osteoarthritis detected by radiography. *Osteoarthr. Cartil.* 12, 10–19.
- Buie, H.R., Campbell, G.M., Klinck, R.J., MacNeil, J.A., Boyd, S.K., 2007. Automatic segmentation of cortical and trabecular compartments based on a dual threshold technique for in vivo micro-ct bone analysis. *Bone* 41, 505–515.

- Burghardt, A.J., Buie, H.R., Laib, A., Majumdar, S., Boyd, S.K., 2010. Reproducibility of direct quantitative measures of cortical bone microarchitecture of the distal radius and tibia by hr-pqct. *Bone* 47, 519–528.
- Burr, D.B., 2004. The importance of subchondral bone in the progression of osteoarthritis. *J. Rheumatol.* 70, 2021.
- Calderazzi, F., Groppi, G., Ricotta, A., Ceccarelli, F., 2014. Does hip osteoarthritis have a protective effect against proximal femoral fractures? A retrospective study. *HIP Int.* 24, 231–236.
- Carballido-Gamio, J., Harnish, R., Saeed, I., Streeter, T., Sigurdsson, S., Amin, S., Atkinson, E.J., Therneau, T.M., Siggeirsdottir, K., Cheng, X., Melton, L.J., Keyak, J., Gudnason, V., Khosla, S., Harris, T.B., Lang, T.F., Carballido-Gamio, J., Harnish, R., Saeed, I., Streeter, T., Sigurdsson, S., Amin, S., Atkinson, E.J., Therneau, T.M., Siggeirsdottir, K., Cheng, X., Melton, L.J., Keyak, J., Gudnason, V., Khosla, S., Harris, T.B., Lang, T.F., 2013. Proximal femoral density distribution and structure in relation to age and hip fracture risk in women. *J. Bone Miner. Res.* 28, 537–546.
- Chan, M.Y., Center, J.R., Eisman, J.A., Nguyen, T.V., 2014. Bone mineral density and association of osteoarthritis with fracture risk. *Osteoarthr. Cartil.* 22, 1251–1258.
- Chen, Y., Hu, Y., Yu, Y.E., Zhang, X., Watts, T., Zhou, B., Wang, J., Wang, T., Zhao, W., Chiu, K.Y., Leung, F.K., Cao, X., Macaulay, W., Nishiyama, K.K., Shane, E., Lu, W.W., Guo, X.E., 2018. Subchondral trabecular rod loss and plate thickening in the development of osteoarthritis. *J. Bone Miner. Res.* 33, 316–327.
- Chiba, K., Burghardt, A.J., Osaki, M., Majumdar, S., 2014. Three-dimensional analysis of subchondral cysts in hip osteoarthritis: an ex vivo HR-PqCT study. *Bone* 66, 140–145.
- Chudyk, A.M., Ashe, M.C., Gorman, E., Al Tunajji, H.O., Crossley, K.M., 2012. Risk of hip fracture with hip or knee osteoarthritis: a systematic review. *Clin. Rheumatol.* 31, 749–757.
- Cooper, D.M., Thomas, C.D.L., Clement, J.G., Turinsky, A.L., Sensen, C.W., Hallgrímsson, B., 2007. Age-dependent change in the 3D structure of cortical porosity at the human femoral midshaft. *Bone* 40, 957–965.
- Cooper, D.M.L., Kawalilak, C.E., Harrison, K., Johnston, B.D., Johnston, J.D., 2016. Cortical bone porosity: what is it, why is it important, and how can we detect it? *Curr. Osteoporos. Rep.* 14, 187–198.
- Crema, M.D., Roemer, F.W., Zhu, Y., Marra, M.D., Niu, J., Zhang, Y., Lynch, J.A., Javaid, M.K., Lewis, C.E., El-Khoury, G.Y., Felson, D.T., Guermazi, A., 2010. Subchondral cystlike lesions develop longitudinally in areas of bone marrow edema-like lesions in patients with or at risk for knee osteoarthritis: detection with mr imaging—the MOST study. *Radiology* 256, 855–862.
- Currey, J.D., 1988. The effect of porosity and mineral content on the Young's modulus of elasticity of compact bone. *J. Biomech.* 21, 131–139.
- Day, J.S., Ding, M., Van Der Linden, J.C., Hvid, I., Sumner, D.R., Weinans, H., Linden, J. C.V.D., Hvid, I., Sumner, D.R., Weinans, H., 2001. A decreased subchondral trabecular bone tissue elastic modulus is associated with pre-arthritis cartilage damage. *J. Orthop. Res.* 19, 914–918.
- Dedrick, D.K., Goldstein, S.A., Brandt, K.O., O'Connor, B.L., Goulet, R.W., Albrecht, M., 1993. A longitudinal study of subchondral plate and trabecular bone in cruciate-deficient dogs with osteoarthritis followed up for 54 months. *Arthritis Rheum.* 36, 1460–1467.
- Ding, M., Odgaard, A.J., Hvid, I., 2003. Changes in the three-dimensional microstructure of human tibial cancellous bone in early osteoarthritis. *J. Bone Joint Surg. (Br.)* 85, 906–912.
- Djuric, M., Zagorac, S., Milovanovic, P., Djonic, D., Nikolic, S., Hahn, M., Zivkovic, V., Bumbasirevic, M., Amling, M., Marshall, R.P., 2013. Enhanced trabecular microarchitecture of the femoral neck in hip osteoarthritis vs. healthy controls: a micro-computer tomography study in postmenopausal women. *Int. Orthop.* 37, 21–26.
- Doube, M., Klosowski, M.M., Arganda-Carreras, I., Cordelières, F.P., Dougherty, R.P., Jackson, J.S., Schmid, B., Hutchinson, J.R., Shefelbine, S.J., 2010. BoneJ: free and extensible bone image analysis in ImageJ. *Bone* 47, 1076–1079.
- Fazzalari, N.L., Kuliwaba, J.S., Forwood, M.R., 2002. Cancellous bone microdamage in the proximal femur: influence of age and osteoarthritis on damage morphology and regional distribution. *Bone* 31, 697–702.
- Fox, K.M., Cummings, S.R., Williams, E., Stone, K., 2000. Femoral neck and intertrochanteric fractures have different risk factors: a prospective study. *Osteoporos. Int.* 11, 1018–1023.
- Friston, K.J., Frith, C.D., Liddle, P.F., Frackowiak, R.S., 1991. Comparing functional (PET) images: the assessment of significant change. *J. Cereb. Blood Flow Metab.* 11, 690–699.
- Ganz, R., Parvizi, J., Beck, M., Leunig, M., Nötzli, H., Siebenrock, K.A., 2003. Femoroacetabular impingement: a cause for osteoarthritis of the hip. *Clin. Orthop. Relat. Res.* 112–120.
- Goldring, S.R., 2008. The role of bone in osteoarthritis pathogenesis. *Rheum. Dis. Clin. N. Am.* 34, 561–571.
- Hartley, A., Hardcastle, S.A., Frysz, M., Parkinson, J., Paternoster, L., McCloskey, E., Poole, K.E.S., Javaid, M.K., Aye, M., Moss, K., Williams, M., Tobias, J.H., Gregson, C. L., 2021. Increased development of radiographic hip osteoarthritis in individuals with high bone mass: a prospective cohort study. *Arthritis Res. Ther.* 23.
- Hayami, T., Pickarski, M., Zhuo, Y., Wesolowski, G.A., Rodan, G.A., Duong, L.T., 2006. Characterization of articular cartilage and subchondral bone changes in the rat anterior cruciate ligament transection and meniscectomized models of osteoarthritis. *Bone* 38, 234–243.
- Javaid, M.K., Lane, N.E., Mackey, D.C., Lui, L., Arden, N.K., Beck, T., Hochberg, M.C., Nevitt, M.C., 2009. Changes in proximal femoral mineral geometry precede the onset of radiographic hip osteoarthritis: the study of osteoporotic fractures HHS public access. *Arthritis Rheum.* 60, 2028–2036.
- Johannesdottir, F., Poole, K.E.S., Reeve, J., Siggeirsdottir, K., Aspelund, T., Mogensen, B., Jonsson, B.Y., Sigurdsson, S., Harris, T.B., Gudnason, V.G., Sigurdsson, G., 2011. Distribution of cortical bone in the femoral neck and hip fracture: a prospective case-control analysis of 143 incident hip fractures; the AGES-REYKJAVIK study. *Bone* 48, 1268–1276.
- Jordan, G.R., Loveridge, N., Bell, K.L., Power, J., Dickson, G.R., Vedi, S., Rushton, N., Clarke, M.T., Reeve, J., 2003. Increased femoral neck cancellous bone and connectivity in coxarthrosis (hip osteoarthritis). *Bone* 32, 86–95.
- Kellgren, J.H., Lawrence, J.S., 1957. Radiological assessment of osteoarthrosis. *Ann. Rheum. Dis.* 16, 494.
- Mansell, J.P., Bailey, A.J., 1998. Abnormal cancellous bone collagen metabolism in osteoarthritis. *J. Clin. Invest.* 101, 1596–1603.
- Marques, E.A., Carballido-Gamio, J., Gudnason, V., Sigurdsson, G., Sigurdsson, S., Aspelund, T., Siggeirsdottir, K., Launer, L., Eiriksdottir, G., Lang, T., Harris, T.B., 2018. Sex differences in the spatial distribution of bone in relation to incident hip fracture: findings from the Ages-Reykjavik study. *Bone* 114, 72–80.
- Mccalden, R.W., McGeough, J.A., Barker, M.B., Court-brown, C.M., McGlough, J.A., Barker, M.B., Court-brown, C.M., 1993. Age-related changes in the tensile properties of cortical bone. The relative importance of changes in porosity, mineralization, and microstructure. *J. Bone Joint Surg. Am.* 75, 1193–1205.
- Messent, E.A., Ward, R.J., Tonkin, C.J., Buckland-Wright, C., 2005. Tibial cancellous bone changes in patients with knee osteoarthritis. A short-term longitudinal study using fractal signature analysis. *Osteoarthr. Cartil.* 13, 463–470.
- Mori, S., Burr, D.B., 1993. Increased intracortical remodeling following fatigue damage. *Bone* 14, 103–109.
- Nawathe, S., Nguyen, B.P., Barzani, N., Akhlaghpour, H., Bouxsein, M.L., Keaveny, T. M., 2015. Cortical and trabecular load sharing in the human femoral neck. *J. Biomech.* 48, 816–822.
- Neil Dong, X., Edward Guo, X., Dong, X.N., Guo, X.E., 2004. The dependence of transversely isotropic elasticity of human femoral cortical bone on porosity. *J. Biomech.* 37, 1281–1287.
- Neilson, M., White, A., Malik, U., Morrison, E., McGill, P.E., McDonald, S.W., 2004. Changes in bone architecture in the femoral head and neck in osteoarthritis. *Clin. Anat.* 17, 378–391.
- Pataky, T.C., 2010. Generalized n-dimensional biomechanical field analysis using statistical parametric mapping. *J. Biomech.* 43, 1976–1982.
- Pataky, T.C., 2016. rft1d: smooth one-dimensional random field upcrossing probabilities in python. *J. Stat. Softw.* 71.
- Pedersen, N.W.N., Schmidt, S.A., Christensen, F., Kjaersgaard-Andersen, P., 1987. Osteoarthritis of the hip in patients with proximal femoral fractures: brief report. *J. Bone Joint Surg. (Br.)* 69-B, 529.
- Poole, K.E.S., Skingle, L., Gee, A.H., Turmezei, T.D., Johannesdottir, F., Blesic, K., Rose, C., Vindlacheruvu, M., Donell, S., Vaculik, J., Dungal, P., Horak, M., Stepan, J. J., Reeve, J., Treece, G.M., 2017. Focal osteoporosis defects play a key role in hip fracture. *Bone* 94, 124–134.
- Radin, E.L., Rose, R.M., 1986. Role of subchondral bone in the initiation and progression of cartilage damage. *Clin. Orthop. Relat. Res.* 213, 34.
- Radin, E., Paul, I., Rose, R., 1972. Role of mechanical factors in pathogenesis of primary osteoarthritis. *Lancet* 299, 519–522.
- Rhaney, K., Lamb, D.W., 1955. The cysts of osteoarthritis of the hip; a radiological and pathological study. *J. Bone Joint Surg. Br. Vol.* 37-B, 663–675.
- Rubinacci, A., Tresoldi, D., Scalco, E., Villa, I., Adorni, F., Moro, G.L., Fraschini, G.F., Rizzo, G., 2012. Comparative high-resolution pQCT analysis of femoral neck indicates different bone mass distribution in osteoporosis and osteoarthritis. *Osteoporos. Int.* 23, 1967–1975.
- Saber Hosnijeh, F., Zuiderwijk, M.E., Versteeg, M., Smeets, H.T., Hofman, A., Uitterlinden, A.G., Agricola, R., Oei, E.H., Waarsing, J.H., Bierma-Zeinstra, S.M., van Meurs, J.B., 2017. Cam deformity and acetabular dysplasia as risk factors for hip osteoarthritis. *Arthritis Rheum.* 69, 86–93.
- Schaffler, M.B., Burr, D.B., 1988. Stiffness of compact bone: effects of porosity and density. *J. Biomech.* 21, 13–16.
- Schindelin, J., Arganda-Carreras, I., Frise, E., Kaynig, V., Longair, M., Pietzsch, T., Preibisch, S., Rueden, C., Saalfeld, S., Schmid, B., Tinevez, J.-Y., White, D.J., Hartenstein, V., Eliceiri, K., Tomancak, P., Cardona, A., 2012. Fiji: an open-source platform for biological-image analysis. *Nat. Methods* 9, 676–682.
- Sugano, M., Hagiwara, S., Nakamura, J., Matsuura, Y., Suzuki, T., Wako, Y., Miura, M., Kawarai, Y., Nawata, K., Yoshino, K., Konno, K., Yoh, S., Ohtori, S., 2020. Comparison study of bone strength of the proximal femur with and without hip osteoarthritis by computed tomography-based finite element analysis. *J. Biomech.* 105, 109810.
- Thomas, G.E., Palmer, A.J., Batra, R.N., Kiran, A., Hart, D., Spector, T., Javaid, M.K., Judge, A., Murray, D.W., Carr, A.J., Arden, N.K., Glyn-Jones, S., 2014. Subclinical deformities of the hip are significant predictors of radiographic osteoarthritis and joint replacement in women. A 20 year longitudinal cohort study. *Osteoarthr. Cartil.* 22, 1504–1510.
- Tomes, J., de Morgan, C., 1853. Observations on the structure and development of bone. *Philos. Trans. R. Soc. Lond.* 143, 109–139.
- Treece, G.M., Gee, A.H., 2015. Independent measurement of femoral cortical thickness and cortical bone density using clinical CT. *Med. Image Anal.* 20, 249–264.
- Treece, G.M., Gee, A.H., Mayhew, P.M., Poole, K.E.S., 2010. High resolution cortical bone thickness measurement from clinical CT data. *Med. Image Anal.* 14, 276–290.
- Treece, G.M., Gee, A.H., Tonkin, C., Ewing, S.K., Cawthron, P.M., Black, D.M., Poole, K.E. S., 2015. Predicting hip fracture type with cortical bone mapping (CBM) in the osteoporotic fractures in men (MrOS) study. *J. Bone Miner. Res.* 30, 2067–2077.
- Turmezei, T.D., Lomas, D.J., Hopper, M.A., Poole, K.E.S., 2014. Severity mapping of the proximal femur: a new method for assessing hip osteoarthritis with computed tomography. *Osteoarthr. Cartil.* 22, 1488–1498.

- Turmezei, T.D., Treece, G.M., Gee, A.H., Fotiadou, A.F., Poole, K.E., S, 2016. In: Quantitative 3D Analysis of Bone in Hip Osteoarthritis Using Clinical Computed Tomography, European Radiology; Heidelberg, 26, pp. 2047–2054.
- Unnikrishnan, G.U., Morgan, E.F., 2011. A new material mapping procedure for quantitative computed tomography-based, continuum finite element analyses of the vertebra. *J. Biomech. Eng.* 133.
- van der Kraan, P.M., van den Berg, W.B., 2007. Osteophytes: relevance and biology. *Osteoarthr. Cartil.* 15, 237–244.
- Wachter, N.J., Krischak, G.D., Mentzel, M., Sarkar, M.R., Ebinger, T., Kinzl, L., Claes, L., Augat, P., 2002. Correlation of bone mineral density with strength and microstructural parameters of cortical bone in vitro. *Bone* 31, 90–95.
- Wahlquist, J.A., DelRio, F.W., Randolph, M.A., Aziz, A.H., Heveran, C.M., Bryant, S.J., Neu, C.P., Ferguson, V.L., 2017. Indentation mapping revealed poroelastic, but not viscoelastic, properties spanning native zonal articular cartilage. *Acta Biomater.* 64, 41–49.
- Wang, B., Overgaard, S., Chemnitz, J., Ding, M., 2016. Cancellous and cortical bone microarchitectures of femoral neck in rheumatoid arthritis and osteoarthritis compared with donor controls. *Calcif. Tissue Int.* 98, 456–464.
- Wolf, O., Ström, H., Milbrink, J., Larsson, S., Mallmin, H., 2009. Differences in hip bone mineral density may explain the hip fracture pattern in osteoarthritic hips. *Acta Orthop.* 80, 308–313.
- Zebaze, R., Ghasem-Zadeh, A., Mbala, A., Seeman, E., 2013. A new method of segmentation of compact-appearing, transitional and trabecular compartments and quantification of cortical porosity from high resolution peripheral quantitative computed tomographic images. *Bone* 54, 8–20.